Discrete Element Modeling of Compound Rockfall Fence Nets

Previtali, Marco; Ciantia, Matteo; Spadea, Saverio; Castellanza, Riccardo ; Crosta, Giovanni B.

Published in:
Challenges and Innovations in Geomechanics

DOI:
10.1007/978-3-030-64518-2_66

Publication date:
2021

Document Version
Peer reviewed version

Discrete element modeling of compound rockfall fence nets

Marco Previtali[1,*], Matteo Ciantia[1], Saverio Spadea[1], Riccardo Castellanza[2] and Giovanni Crosta[2]

[1] School of Science and Engineering, University of Dundee
Nethergate, Dundee DD1 4HN, (UK)
m.previtali@dundee.ac.uk

[2] Department of Earth and Environmental Sciences (DISAT), Università di Milano-Bicocca
Piazza della Scienza, 4, 20126 Milano (Italy)

Abstract Compound mesh panels are structures in which two different nets geometries are employed: a main mesh that provides the bearing capacity and a weaker mesh with a thin sieve size to catch smaller blocks that can pass through otherwise. Typically, only the effect of the main mesh is investigated, and the weaker mesh is considered to provide negligible structural resistance. In this paper, after a calibration procedure, numerical simulations of quasi-static punch tests and a dynamic block impact on a composite double-twist and strand rope mesh are performed. The results show that, under dynamic conditions, the presence of the finer mesh lowers the peak force acting on the main mesh. This effect is not found under quasi-static conditions and has important repercussions on the overall structural resistance as the energy dissipation mechanism reduces the stress on the mesh fence posts.

Keywords: Discrete Element Modelling; Punch test; Impact test; Rockfall risk mitigation; Stress repartition

1 Introduction

Flexible net barriers and drapery meshes are the most widespread structures used for the mitigation of rockfall hazard. They are characterized by a complex mechanical behavior due to the concurring effects of large inertial deformations, contact interactions and non-linear material response. These structures are typically tested using either well-established quasi-static tensile and punching tests, or experimental dynamic impact tests, without bridging between the two approaches (Bertolo et al., 2009; Gao, et al., 2018; Mentani et al., 2018) . The studies that investigate the influence of additional net elements on the mesh are limited to longitudinal cables (Albaba et al., 2017; Mentani et al., 2018). Herein, a discrete element method (DEM) numerical model of mesh panels, following the remote contact approach by Nicot et al., (2001); is calibrated using experimental data from the literature. The calibrated DEM model is then employed to

This is a post-peer-review, pre-copyedit version of an article published in *Lecture Notes in Civil Engineering*, vol. 126. The final authenticated version is available online at: https://doi.org/10.1007/978-3-030-64518-2_66.

investigate the force repartition on the different mesh elements and the effect of adding different mesh panels under both quasi-static and dynamic tests. The compound (or double) mesh investigated is composed by a hexahedral double-twisted mesh and a strand-rope square mesh. The former is the cheapest and most widespread mesh type used for its small sieve size and its ability to maintain its shape after failure, due to the frictional interaction of double-twist interweavements, which is not present in chain-link meshes, the other commonly employed small sieve size meshes. Strand-rope meshes are widespread due to their low bending stiffness, which allows for cheap transport and installation procedures when compared to steel-ring meshes.

2 Discrete element representation of wire meshes

The hexahedral and square mesh panels are represented by a set of discrete element spheres connected by remote interactions. Since these bonds are not physical entities, net-boulder contact resolution is only carried out on the spheres, whose density is set to an arbitrary value so that the mass of the virtual mesh panel is equivalent to the real one. Implementation details for the hexahedral double-twisted mesh can be found in Thoeni et al., (2013). Gabrieli et al., (2017) showed that, for the interaction with large objects such as the punch-test platter, this type of simplified remote-bond approach produces the same results as the one where contact detection is carried out on the wire geometry. The models presented in the above-mentioned papers consider purely tensional truss-like bond behavior, which assumes that the bending and compressive stiffness of a wire is negligible due to the immediate onset of buckling. While this assumption is reasonable when considering thin cables, it may not when as the wire section increases. Herein, a more physically consistent bending stiffness is implemented through the parallel bond contact model (Potyondy et al., 2004), which applies tensile and shear stresses following classic beam theory. To validate the model, a numerical simulation of a beam tip loading bending test is performed and compared with analytical solutions. The cylindrical beam considered is 2 meters long, with 1 cm section and characterized by a Young modulus, $E = 10$ GPa and Poisson ratio, $\nu = 0.288$. A comparison of the numerical results with the analytical solution is presented in Fig. 1. All simulations were run using the Particle Flow Code software (PFC3D) by Itasca, (2010), which considers dynamic interactions between rigid bodies following classic DEM theory.

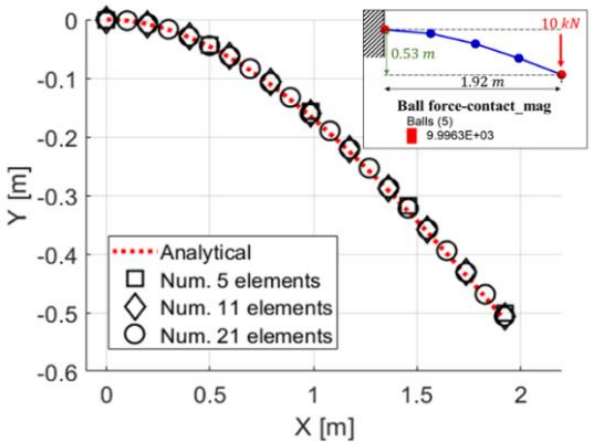

Figure 1: Comparison of the numerical results and the analytical solution for a beam loading test. Tests with a 5, 11 and 21 elements beam have been carried out. The maximum error is found with the 5 elements beam, in which the normalized RMSE value is less than 2.5%. On the top-right, a view of the numerical model.

3 Test setup

The punching test setup employed herein is chosen due to the availability of experimental results for strand rope square-meshes (Bonati et al., 2004) and the existence of a previously calibrated numerical model for hexagonal meshes (Pol et al., 2017). For hexagonal meshes, Bertrand et al, (2008) produced both an experimental dataset and a numerical model of a punch test. However, we did not employ this dataset because no information on the platter size used for the physical test was provided. Furthermore, in the numerical model, instead of the typical semi-spheroid geometry, they employed a sphere, characterized by larger curvature. This causes the mesh-platter contact area to increase at a lower rate, modifying the test.

For all punch tests, the net panel is pinned on all sides and indented by a displacing a platter, upon which the reaction force is measured, at a velocity of 1 cm/sec. For the hexagonal meshes, the standardized semi-spheroid platter geometry presented in Pol et al., (2017) is employed, while a conic geometry is employed for the square mesh, following Bonati et al., (2004). Finally, as the pre-loading conditions of the panel for the literature tests are unknown, here the panel was pre-loaded by blocking the movement of the discrete elements at the net extremities along the gravity direction and pulling until a maximum vertical displacement of 1 cm was achieved in the center. The last degree of freedom was maintained, and the elements were free to move along the edges of the mesh to avoid the generation of localized stress at the corners. For the dynamic impact tests, the net geometry and properties were the same as for the punch test. The boulder is constituted by a 45 cm side truncated cube, 44.5 kg in mass, following the

European guidelines (EOTA, 2013). The impact velocity was fixed to 10 m/s. The test geometrical details are listed in Table 1.

Table 1 Punch test specifications.

			Net Element Size [mm]		Platter geometry [m]	
Study	Panel Size [m]	Wire Section [mm]	Axis 1	Axis 2	Radius	Height
Pol et al., 2017	3	2.7	100	80	0.5	0.15
Bonati et al., 2004	3	10	300	300	0.34	0.78

4 Model calibration and test execution

Pol et al, (2017) employed the stochastically distorted mesh model proposed by Thoeni, et al (2013). This model employs two separate stress-strain curves for the single-wire (SW) and double-twist (DT) interactions, obtained experimentally. Successively, due to the non-homogeneous plasticization of the wire-mesh, the curve applied to each contact is translated along the strain axis following a random distribution and two model fitting parameters. Thoeni et al., (2013) calibrated the model on quasi-static pulling tests and a dynamic impact test, considering an average curve translation of 10% strain, while Pol et al., (2017), for quasi-static punch tests, used a value of 1%, which provides a stiffer response. For simplicity, we decided to remove the stochastic model altogether, setting a 0% value. Regarding the square mesh wires, Albaba, et al., (2017) modelled the experimental punch test from Bonati e al., (2004) with a pure elastic wire model ($E_n = 60\,GPa\,, \nu = 0.3$). Therein, the wires were implemented following the approach by Effeindzourou et al., (2017), meaning they adopted classical beam theory for bending and twisting moments and the wires can be seen as a sum of cylinders. We chose to employ the same value for the Young Modulus as it is consistent with values typically reported in the literature (Bertrand et al., 2012; Mentani et al., 2016). We did not introduce a steel plasticity model as strand ropes exhibit very limited plastic behavior and a low value of localized strain is achieved on the contact bonds (Kalentev et al., 2017; Wang et al., 2015). All the calibration procedures and tests were carried out with a linear contact model between the platter / boulder and the mesh, as listed in **Table 1**. For the dynamic tests, energy dissipation was accounted for through local damping on the DEM elements (Damping factor = 0.5 [-], following Thoeni et al., (2013)). No damping is applied to the impacting boulder.

Table 1: Mesh-platter/boulder contact parameters for all the tests carried out

Parameter	Normal stiffness (kn)	Shear stiffness (ks)	Friction
Value	1e9 [N/m]	1e8 [N/m]	0.2 [-]

Finally, in absence of a complete description of the strand wire type, the bending moment of the wire, after being calibrated on the punch test results, was expressed here as the ratio between its bending stiffness and that of a cylindric beam with equivalent section. Only five simulation results are shown for brevity (see **Table 2**).

Table 2: Steel strand rope model specifics for the numerical square mesh punching test

Simulation Index	1	2	3	4	5
Bending Stiffness Ratio	0.0	0.01	0.05	0.25	1.0

Figure 3 shows that the best fitting was obtained for steel wires characterized by 5% of bending stiffness of the equivalent section cylindric beams. Additionally, the influence of this parameter decreases progressively.

After calibration, a punch test on both a hexagonal double-twist mesh and a composite hexagonal plus square mesh using the semi-spheroid geometry was carried out. During the test, the total and maximum tensile forces in the remote bonds within a circular area with radius of one meter, located at the center of the mesh panel were monitored. This was done to investigate the behavior of the mesh in proximity of the contact with the platter. The same was done for the impact tests.

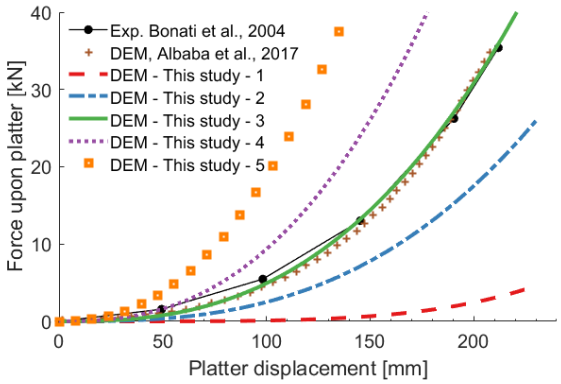

Figure 2: Force-displacement curves for the numerical punch tests carried out on the square mesh using the cone geometry.

5 Results and discussion

The results for the punching tests are plotted in Figure 3, while Figure 4 shows the test during its execution. Both the double net and hexagonal mesh plots exhibit similar trends and we assume the difference was caused by the pre-loading conditions (the double mesh has much stiffer contacts due to the presence of the strand rope, meaning the hexahedral mesh is less loaded at the beginning of the punch test). It is seen that DT

interactions are the most loaded individually (Figure 3a) but contribute less to the total mesh capacity (Figure 3b). The strand-rope tensile force-platter displacement curve exhibits no significant differences from the one in Figure 3, reaching a value of 22.5 [MN] for the total force and 11.5 [kN] for the maximum individual bond force. These plots are not included for brevity.

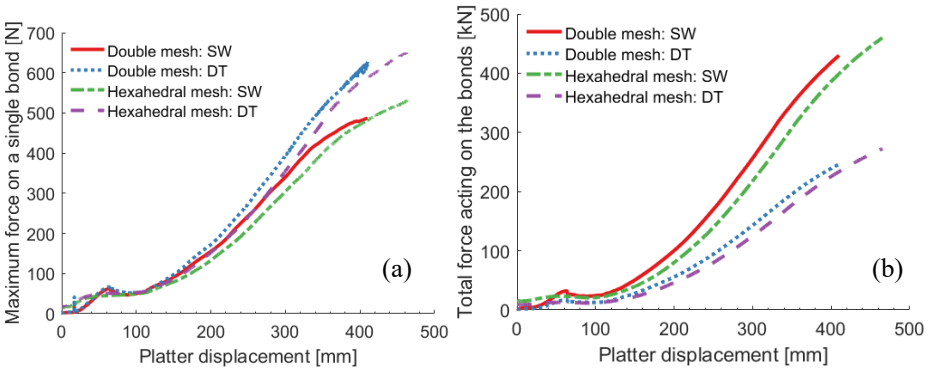

Figure 3: Tensile force in the mesh during the test, subdivided per element type: double-twist (DT) and single-wire (SW).

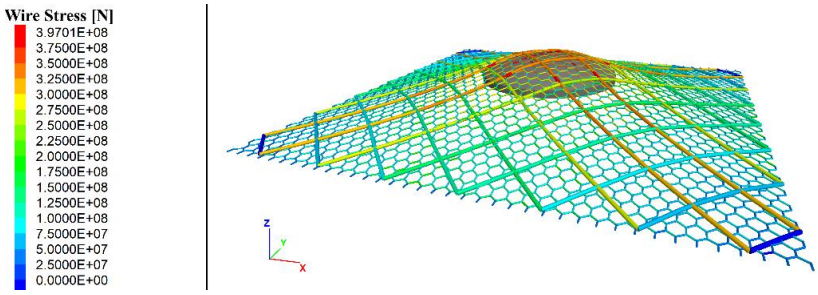

Figure 4: Punch test on the composite strand rope square mesh + hexagonal double twist mesh. Contacts are coloured by axial tensile stress magnitude.

The impact test results (Figure 5) show the same overall trend as during quasi-static punch tests, with the single-wire contacts bearing most of the total load and double-twist interactions achieving higher individual contact force. During the first impact (i.e. t = 0 [s]), the total force acting on the strand rope mesh is equal to the force acting on the single wire contacts for the non-composite hexahedral mesh simulation (500 kN, Hexahedral mesh: SW). The maximum force acting on double-twist interactions during the first impact appears to be significantly higher than that acting on the square mesh, as the hexahedral mesh is solicited first, while this effect disappears during the second impact.

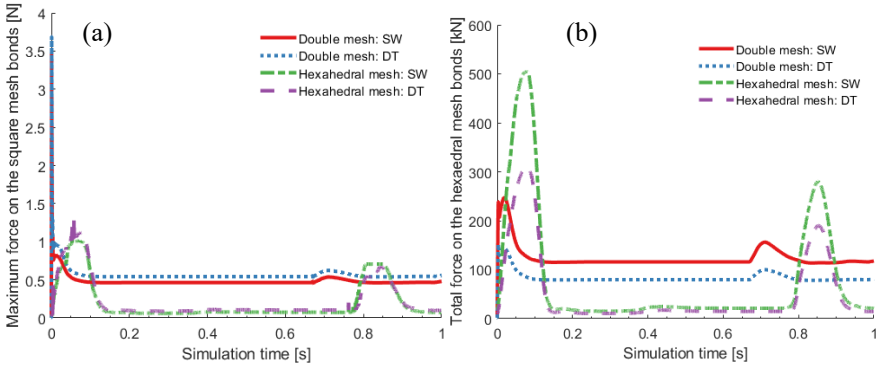

Figure 5: Force repartition on the hexagonal mesh wires during the impact tests.

Figure 6 compares the force acting on a strand rope square mesh when the hexagonal mesh is not present to when it is. The peak force is approximatively 1 MN higher in the former scenario. As shown by the successive rebounds (t = 0.25 s and t = 0.7 s), the maximum force is similar for both mesh configurations, while the total force is higher for a pure square mesh.

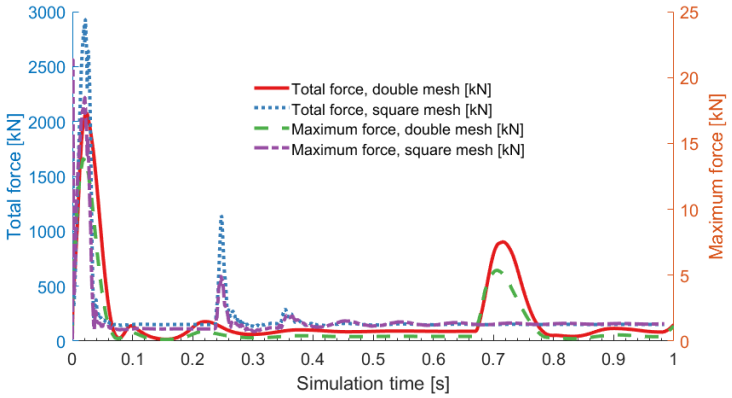

Figure 6: Force repartition on the square mesh wires during the impact tests.

6 Concluding remarks

This paper presents a set of numerical simulations of both quasi-static and dynamic impact tests on different mesh panels. The behaviour of the strand-rope mesh has been implemented considering its bending stiffness as a fraction of that of an equivalent section area cylindrical beam. During both quasi-static and dynamic conditions, double-twist interactions bear the maximum load, while the overall capacity of the mesh

depends on single-wire contacts. For the impact tests, the presence of the strand rope mesh in the compound structure halves the peak for the total force acting on the wires, but not for the maximum force, which can cause local failure on the contact position. At the same time, the presence of the hexagonal mesh lowers the peak force in the square mesh panel, which in turn decreases the load acting on the fence posts.

References

Bendat, J.S., and Piersol, A.G. (2000). *Random Data: Analysis and Measurement Procedures*. Third edn. John Wiley & Sons, Ltd.

Albaba, A., Lambert, S., Kneib, F., Chareyre, B., & Nicot, F. (2017). DEM Modeling of a Flexible Barrier Impacted by a Dry Granular Flow. *Rock Mechanics and Rock Engineering*, 50(11), 3029–3048.

Bertolo, P., Oggeri, C., & Peila, D. (2008). Full-scale testing of draped nets for rock fall protection.

Bertrand, D., Trad, A., Limam, A., & Silvani, C. (2012). Full-scale dynamic analysis of an innovative rockfall fence under impact using the discrete element method: From the local scale to the structure scale. Rock Mechanics and Rock Engineering, 45(5), 885–900.

Bertrand, D., Nicot, F., Gotteland, P., & Lambert, S. (2008). Discrete element method (DEM) numerical modeling of double-twisted hexagonal mesh. Canadian Geotechnical Journal, 45(8), 1104–1117.

Bonati, A., & Galimberti, V. (2004). La valutazione sperimentale di sistemi di difesa attiva dalla caduta massi. Bonifica Dei Versanti Rocciosi per La Protezione Del Territorio, 11–12.

Effeindzourou, A., Thoeni, K., Giacomini, A., & Wendeler, C. (2017). Efficient discrete modelling of composite structures for rockfall protection. *Computers and Geotechnics*, 87, 99–114.

EOTA. (2013). ETAG 027:2013 Falling Rock Protection Kits. (December 1988).

Gabrieli, F., Pol, A., & Thoeni, K. (2017). Comparison of two DEM strategies for modelling cortical meshes.

Gao, Z., Al-Budairi, H., & Steel, A. (2018). Experimental testing of low-energy rockfall catch fence meshes. *Journal of Rock Mechanics and Geotechnical Engineering*, 10(4), 798–804.

Itasca. (2010). Particle flow code in three dimensions: Software manual. Minnesota, MN, USA.

Kalentev, E., Václav, Š., Božek, P., Korshunov, A., & Tarasov, V. (2017). Numerical analysis of the stress-strain state of a rope strand with linear contact under tension and torsion loading conditions. *Advances in Science and Technology Research Journal*, 11(2), 231–239.

Mentani, A., Govoni, L., Giacomini, A., Gottardi, G., & Buzzi, O. (2018). An Equivalent Continuum Approach to Efficiently Model the Response of Steel Wire Meshes to Rockfall Impacts. *Rock Mechanics and Rock Engineering,* 51(9), 2825–2838.

Mentani, A, Govoni, L., Gottardi, G., Lambert, S., Bourrier, F., & Toe, D. (2016). A New Approach to Evaluate the Effectiveness of Rockfall Barriers. *Procedia Engineering*

Nicot, F., Cambou, B., & Mazzoleni, G. (2001). Design of Rockfall Restraining Nets from a Discrete Element Modelling. Rock Mechanics and Rock Engineering, 34(2), 99–118.

Pol, A., Thoeni, K., & Mazzon, N. (2017). Discrete element modelling of punch tests with a double-twist hexagonal wire mesh.

Potyondy, D. O., & Cundall, P. A. (2004). A bonded-particle model for rock. *International Journal of Rock Mechanics and Mining Sciences*, 41(8), 1329–1364.

Thoeni, K., Lambert, C., Giacomini, A., & Sloan, S. W. (2013). Discrete modelling of hexagonal wire meshes with a stochastically distorted contact model. *Computers and Geotechnics*

Wang, X. Y., Meng, X. B., Wang, J. X., Sun, Y. H., & Gao, K. (2015). Mathematical modeling and geometric analysis for wire rope strands. *Applied Mathematical Modelling*